




Article

Morphology and Crystal Structure of $\text{Cu}_2\text{NiSn}(\text{S},\text{Se})_4$ Thin Films Obtained by an Electrodeposition-Annealing Process

Aliona V. Stanchik ^{1,2,*}, Tatsiana N. Asmalouskaya ², Vladimir V. Rakitin ³, Valery F. Gremenok ^{1,2}, Mikhail V. Gapanovich ³, Ekaterina L. Trukhanova ^{1,*}, Tatiana I. Zubar ¹ , Alex V. Trukhanov ¹  and Sergei V. Trukhanov ¹ 

¹ Scientific and Practical Materials Research Center, National Academy of Sciences of Belarus, 220072 Minsk, Belarus

² Department of Information and Computer Systems Design, Belarusian State University of Informatics and Radioelectronics, 220013 Minsk, Belarus

³ Institute of Problems of Chemical Physics, Russian Academy of Sciences, 142432 Chernogolovka, Russia

* Correspondence: alena.stanchik@bk.ru (A.V.S.); el_trukhanova@mail.ru (E.L.T.)

Abstract: Today, an actual task of photovoltaics is the search for new light-absorbing materials for solar cells, which will make them more efficient and economically affordable. Semiconductor $\text{Cu}_2\text{NiSn}(\text{S},\text{Se})_4$ (CNTSSe) thin films are promising materials due to suitable optical and electrical properties. This compound consists of abundant, inexpensive, and low-toxicity elements. However, few results of studying the properties of CNTSSe films have been presented in the literature. This paper presents the results of studying the morphology, phase composition, and crystal structure of the CNTSSe films, which were first obtained by high-temperature annealing of electrodeposited Ni/Cu/Sn/Ni precursors on glass/Mo substrates in chalcogen vapor. The films were studied using X-ray diffraction, scanning electron microscopy, and energy-dispersive X-ray spectroscopy. It has been found that sequential electrochemical deposition makes it possible to obtain the Ni/Cu/Sn/Ni precursors of the required quality for further synthesis of the films. It is shown that high-temperature annealing in chalcogen vapor in air makes it possible to synthesize stable polycrystalline CNTSSe films. The obtained results confirm that the production of CNTSSe films is suitable for use in solar cells by the proposed method, which can be improved by more precise control of the precursor composition and annealing conditions.

Keywords: metal precursors; electrodeposition; annealing; chalcogen; CNTSSe; thin films; morphology; crystal structure



Citation: Stanchik, A.V.; Asmalouskaya, T.N.; Rakitin, V.V.; Gremenok, V.F.; Gapanovich, M.V.; Trukhanova, E.L.; Zubar, T.I.; Trukhanov, A.V.; Trukhanov, S.V. Morphology and Crystal Structure of $\text{Cu}_2\text{NiSn}(\text{S},\text{Se})_4$ Thin Films Obtained by an Electrodeposition-Annealing Process. *Coatings* **2022**, *12*, 1198. <https://doi.org/10.3390/coatings12081198>

Academic Editor: Heping Li

Received: 20 July 2022

Accepted: 14 August 2022

Published: 17 August 2022

Publisher's Note: MDPI stays neutral with regard to jurisdictional claims in published maps and institutional affiliations.



Copyright: © 2022 by the authors. Licensee MDPI, Basel, Switzerland. This article is an open access article distributed under the terms and conditions of the Creative Commons Attribution (CC BY) license (<https://creativecommons.org/licenses/by/4.0/>).

1. Introduction

Today, the most common solar cells (SCs) are based on silicon and thin films of copper indium gallium selenide and cadmium-telluride due to their high efficiency [1]. However, silicon solar cells have one of the highest costs due to the difficult and energy-intensive manufacturing technology [2]. The copper indium gallium selenide and cadmium-telluride thin films are composed of toxic, low abundant raw materials, and expensive elements. This is predicted to severely limit the production, mass deployment, and economic sustainability of SCs [3,4]. Thin films based on earth-abundant, inexpensive, and low-toxicity elements, specifically $\text{Cu}_2\text{ZnSnS}_4$, $\text{Cu}_2\text{ZnSnSe}_4$, and $\text{Cu}_2\text{ZnSn}(\text{S},\text{Se})_4$ solid solutions, have been extensively researched as absorber materials in recent years [5,6]. These compounds have attracted much attention due to their optimum optical band gap values (about 1.0–1.5 eV) and high absorption coefficients ($\sim 10^4 \text{ cm}^{-1}$) for potential application in thin-film SCs [5,6]. The efficiency of SCs based on $\text{Cu}_2\text{ZnSnSe}_4$, $\text{Cu}_2\text{ZnSnS}_4$, and $\text{Cu}_2\text{ZnSn}(\text{S},\text{Se})_4$ films is 11.95% [7], 11.0%, and 12.6% [1], respectively, with a theoretical possible efficiency of about 30% [8]. The low open-circuit voltage and fluctuations in the band gap of the $\text{Cu}_2\text{ZnSn}(\text{S},\text{Se})_4$ films due to their structure and narrow single-phase region of existence

are the causes of the low efficiency of SCs [9,10]. It is assumed that a large number of anti-structural defects are formed in the films due to the proximity of the ionic radius of Zn^{2+} and Cu^+ . These defects cause disorder in the $\text{Cu}_2\text{ZnSn}(\text{S,Se})_4$ crystal lattice and act as photogenerated current carrier traps. To overcome this problem, it is proposed to replace Zn with another chemical element with the same valency such as Mn, Fe, Co, and Ni. $\text{Cu}_2\text{NiSn}(\text{S,Se})_4$ (CNTSSe), one of the semiconductor materials, has recently received a lot of interest. Theoretical calculations affirm that the substitution of Zn with Ni in the CZTS compound could potentially enhance electrical conductivity and reduce the optical band gap [11]. There are several works on CNTSSe solid solutions in the literature, most of which relate to the synthesis and study of films based on pure sulfur (CNTS). In [12,13] the spin coating method was used to create thin films of CNTSSe nanocrystals on glass substrates. The XRD analysis exhibited the formation of a kesterite phase with peaks corresponding to polycrystalline CNTSSe with a tetragonal structure. The direct band gap and absorption coefficient of the film were 1.29 eV and over 10^4 cm^{-1} , respectively. Two SCs based on CNTS films have been reported: a device glass/Mo/CNTS/CdS/Al-ZnO/Al with 0.09% efficiency [14] and another structure of ITO/ZnO/ZnS/CNTS/Au was 2.71% [15]. An efficiency of 17.06% of SCs based on CNTS films with the CNTS/ZnS/Zn(O,S)/FTO structure has been reported, which was calculated using a solar cell capacitance simulator (SCAPS) program with an illumination spectrum of 1.5 AM [16]. As can be seen, few data on the synthesis and study of solid-solution CNTSSe films have been presented in the literature.

Therefore, this paper presents the results of a study of the morphology, phase composition, and crystal structure of the CNTSSe films. The CNTSSe films were obtained by a non-vacuum two-stage method, where, in the first stage, metal precursors were obtained by electrochemical deposition, and in the second stage, they were annealed in chalcogen vapor at high temperatures. Electrochemical methods are of particular interest to obtain semiconductor thin films due to their scalability and potential low cost compared to vacuum methods [9,17–19]. A two-stage electrochemical deposition method was used to successfully produce $\text{Cu}(\text{In,Ga})(\text{S,Se})_2$ thin films [20]. The efficiency of the solar cell and the module based on them was 17.3% and 14.0%, respectively [20].

2. Materials and Methods

2.1. Synthesis of Thin Films

The CNTSSe thin films were fabricated by the two-step method. In the first step, the Ni/Cu/Sn/Ni precursors were obtained by the sequential electrochemical deposition of metallic layers of nickel, copper, tin, and nickel (Ni/Cu/Sn/Ni) on a glass/Mo substrate in galvanostatic mode. A reasonable order of metal layers in a Cu–Sn–Ni(Zn) precursor for the synthesis of $\text{C}(\text{N,Z})\text{T}(\text{S,Se})$ films is substrate/Cu/Sn/Ni(Zn). However, the copper deposited on the molybdenum sublayer had bad adhesion in this work. A similar behavior of electrochemically deposited copper on a molybdenum layer was observed in [21,22]. Therefore, nickel was used as a sublayer for copper [23] and as a top layer to prevent the loss of volatile tin during subsequent high-temperature annealing. The Ni layers were deposited from aqueous solutions containing NiSO_4 , NiCl_2 , H_3BO_3 , and organic additives with $\text{pH} \approx 3.5\text{--}4$ at $T \approx 50 \text{ }^\circ\text{C}$ and the cathodic current density of $J_c = 20 \text{ mA/cm}^2$ (sublayer) and 25 mA/cm^2 (top layer). The Cu layers were deposited from an aqueous solution containing CuSO_4 , $\text{K}_4\text{P}_2\text{O}_7$, Na_2HPO_4 , and $\text{KNaCuH}_2\text{O}_6$ with $\text{pH} \approx 8\text{--}8.5$ at $T \approx 40 \text{ }^\circ\text{C}$ and the cathodic current density of $J_c = 8 \text{ mA/cm}^2$. The Sn layers were deposited from an aqueous solution of SnSO_4 and H_2SO_4 at room temperature and the cathodic current density of $J_c = 10 \text{ mA/cm}^2$.

The second step is high-temperature annealing of the deposited Ni/Cu/Sn/Ni precursors in chalcogen (sulfur and selenium) vapors in the air. The Ni/Cu/Sn/Ni precursors were annealed at $580 \text{ }^\circ\text{C}$ for 30 min in the one-zone tube furnace. Then, they were naturally cooled in a furnace to room temperature. The precursors, selenium, and sulfur powder were loaded in a quartz box and inserted in the furnace. Selenium and sulfur powder were the sources of chalcogen.

2.2. Characterization Methods

The microphotographs and elemental composition of the fabricated samples were obtained using scanning electron microscopy (SEM) and X-ray spectral microanalysis (EDX) on a ZEISSEVO (Zeiss, Oberkochen, Germany). The phase composition and crystalline structure of the films were studied using an X-ray diffractometer (XRD) D8 Advance (Bruker AXS, Billerica, MA, USA) with $\text{CuK}\alpha$ radiation. Analysis of the phase composition was performed with the use of the Crystallography Open Database (COD) in the “Match” program. For study, the lattice parameters of the films were used with the Rietveld analysis, implemented in the “FullProf” program.

3. Results and Discussion

3.1. Analysis of Morphology of Precursors

For the synthesis of the CNTS_{Se} films, Ni/Cu/Sn/Ni precursors with elemental compositions such as Cu—15.9 at.%, Sn—20.5 at.%, and Ni—63.6 at.% with a total thickness of 700–900 nm were used (Figure 1). The EDX mapping images of the cross-section of the precursors in Figure 1 showed mutual diffusion of the deposited metals, which may indicate the formation of binary and/or ternary intermetallic compounds [21,24]. For example, it was noted in [25] that the $\text{Cu}_{6,26}\text{Sn}_5$ (or Cu_6Sn_5) phase in the Cu–Zn–Sn electrodeposited precursors could form at room temperature. Copper and nickel are completely miscible in both the liquid and solid states [26]. Cu–Ni alloys crystallize over the whole concentration range [26]. In addition, the observed diffusion confirmed good adhesion between the deposited metal layers as well as to the substrate. Nevertheless, two regions could be distinguished on the EDX mapping image of Ni (Figure 1), where Ni diffused throughout the thickness of the precursor (right image area) and two Ni layers were visible (left image area): a sublayer and a top layer.

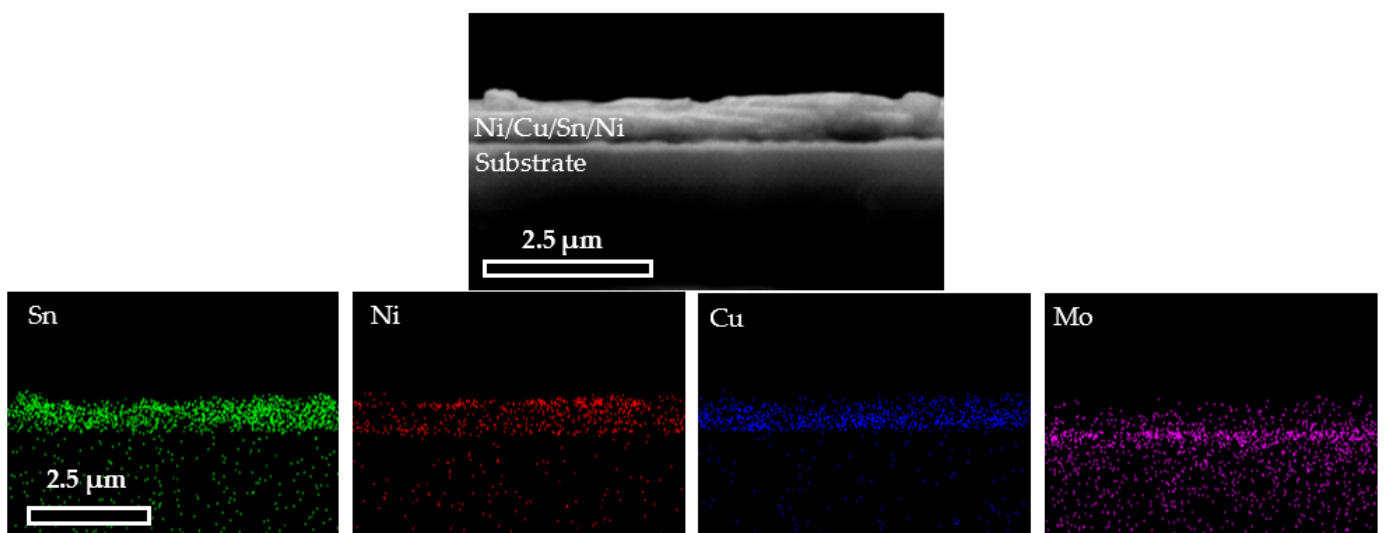


Figure 1. The SEM and EDX mapping images of the cross-section of the Ni/Cu/Sn/Ni precursors on a glass/Mo substrate.

The electrodeposited metal layers of the precursors had a uniform distribution over the surface (Figure 2). However, as can be seen from the EDX mapping images (Figure 2), there were several small dark regions on the tin map (highlighted in white), while in these regions, the distribution of copper and nickel was uniform. These dark regions were depleted in tin due to the technology of the electrochemical deposition of tin from aqueous electrolytes or the aggregation of Ni and Cu metals.

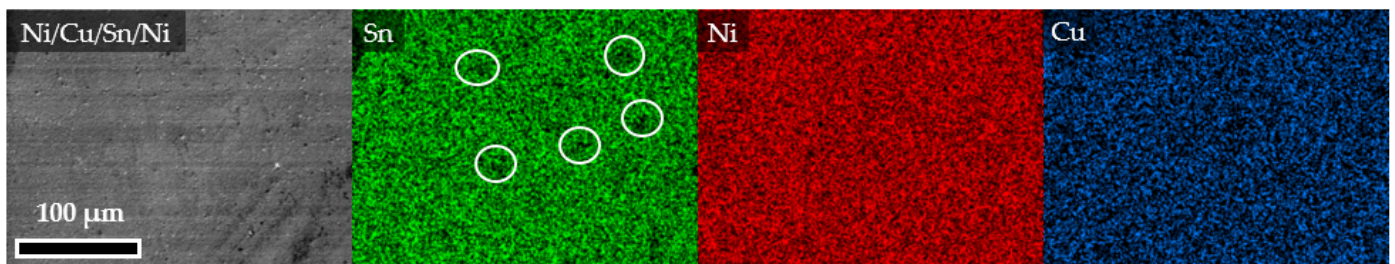


Figure 2. The top view of the SEM and EDX mapping images of the Ni/Cu/Sn/Ni precursors.

3.2. Analysis of Morphology of Thin Films

The elemental composition of the synthesized CNTSSe films is presented in Table 1. The elemental composition of the films was close to the stoichiometric ratio. However, the Cu/(Ni + Sn) and Ni/Sn ratios indicated a deficiency of copper and nickel in the films. In addition, the films were enriched in chalcogen (chalcogen/metal ≈ 1.3). The EDX spectrum of the synthesized CNTSSe films indicated the absence of impurity elements, particularly oxygen, in their composition (Figure 3).

Table 1. The elemental composition and atomic ratio of the CNTSSe thin films.

Elemental Composition, at.%					Ratio		
Cu	Ni	Sn	Se	S	Cu/(Ni + Sn)	Ni/Sn	S/(S + Se)
20.20	11.60	12.47	22.72	33.00	0.84	0.93	0.59

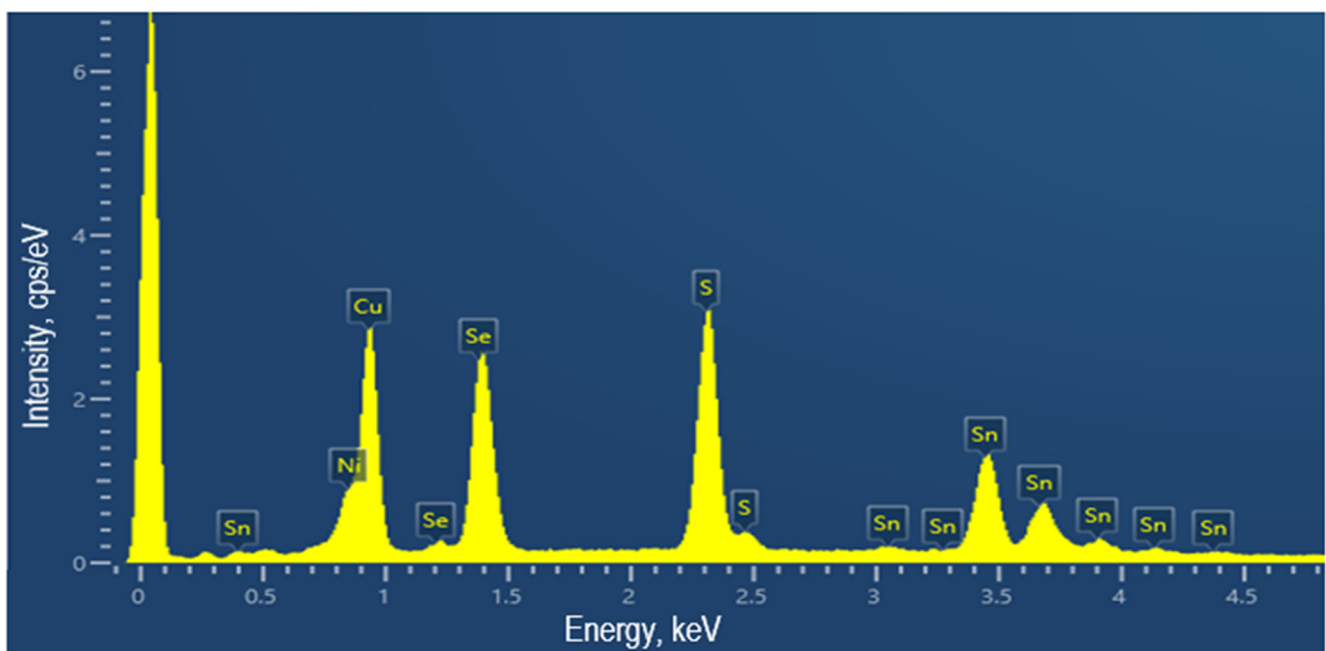


Figure 3. A typical EDX spectrum CNTSSe thin films on a glass/Mo substrate.

Figure 4 shows typical SEM images of the surface and cross-section of the CNTSSe thin films. As can be seen (Figure 4a), the surface of the film was a homogeneous structure without cracks and with densely packed faceted crystals and single pores. The size of the crystals on the surface of the films was greater than one micron, which agglomerated in large grains. Large crystals in the form of stretched petals upward surrounded the pores on the surface of the film. From the cross-sectional images (Figure 4b), the thickness of the films was about 2.4 μm . This value was three times the thickness of the Ni/Cu/Sn/Ni precursors due to the insertion of S and Se atoms in the crystal lattice.

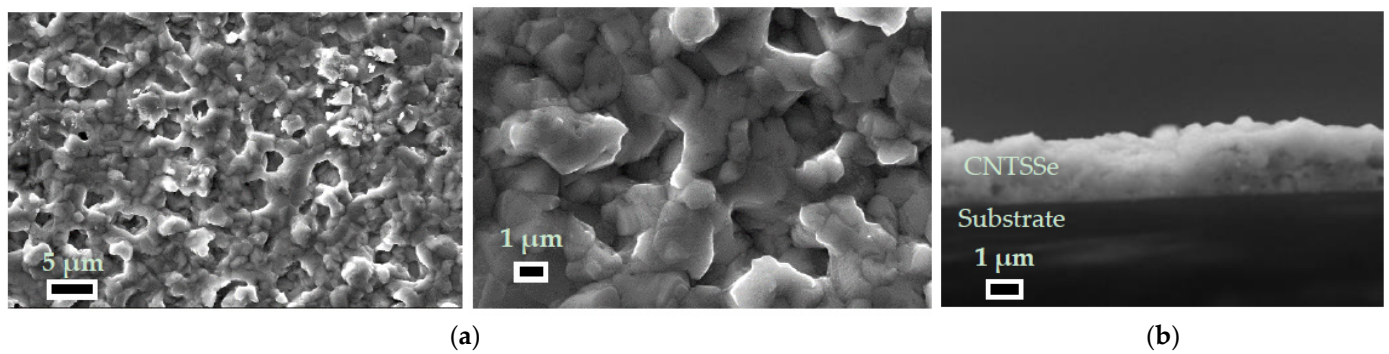


Figure 4. The top view (a) and cross-section (b) SEM mapping images of the CNTSSe thin films on a glass/Mo substrate.

The EDX mapping images of the CNTSSe films showed that the small grains clustered (highlighted in white) on the surface of the films were Ni-rich, Sn-, Cu-, and S-poor while Se was distributed evenly over all of the investigated surfaces (Figure 5). Nevertheless, all constituent elements had a uniform distribution over the surface of the film.

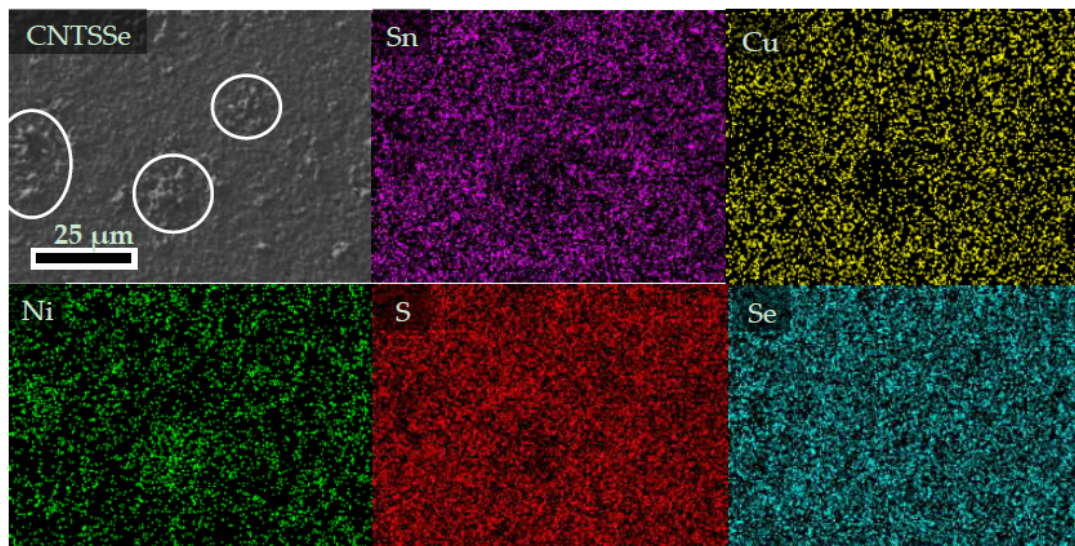


Figure 5. The top view SEM and EDX mapping images of the CNTSSe thin films.

3.3. X-Ray Analysis of Thin Films

A typical X-ray spectrum of the CNTSSe films obtained on glass/Mo substrates is shown in Figure 6. The X-ray diffraction pattern for the films indicated their polycrystalline nature and demonstrated intense peaks (111), (200), (220), and (311) at $2\theta \approx 27.97^\circ$, 32.93° , 46.48° , and 55.10° , respectively. Peaks (111), (220) and (311), as can be seen from Figure 6, were between the positions of the diffraction reflections from cubic CNTSe (COD no. 00-026-0551) and CNTS (COD no. 00-026-0552) of the space group $F-43m$. The crystal structure of the CNTSSe compound was similar to that of CNTSe and CNTS, but due to a change in the lattice parameters, its reflections in the X-ray diffraction patterns were shifted. The low intensity reflection at $2\theta \approx 32.93^\circ$ corresponded to the CNTS phase. These XRD results indicate the formation of an ordered CNTSSe solid solution of a cubic crystal structure. In most works on the synthesis of the CNTS films [27–29], it has been found that the films crystallize in a cubic structure. However, it has been reported that the CNTS and CNTSe films have a wurtzite crystalline structure [30,31]. Moreover, the CNTS and CNTSSe films were obtained with a tetragonal crystalline structure [13,32,33].

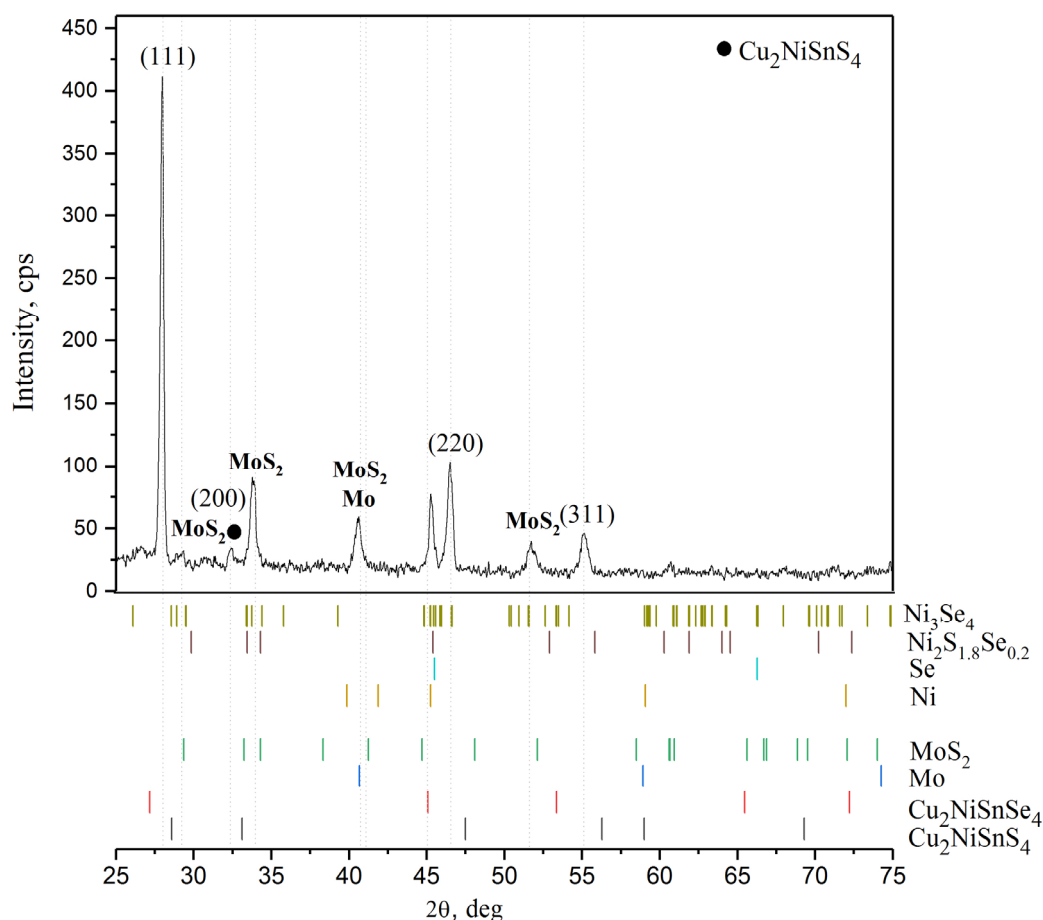


Figure 6. A typical X-ray pattern of the CNTSSe thin films on a glass/Mo substrate. Reference patterns from COD: Ni_3Se_4 (no. 96-900-9245), $\text{Ni}_2\text{S}_{1.8}\text{Se}_{0.2}$ (no. 96-153-8792), Se (no. 96-901-3135), Ni (no. 96-901-3008), MoS_2 (no. 96-153-5541), Mo (no. 96-901-1607), $\text{Cu}_2\text{NiSnSe}_4$ (no. 00-026-0551), $\text{Cu}_2\text{NiSnS}_4$ (no. 00-026-0552).

The X-ray diffraction pattern of the CNTSSe films clearly showed a shift of the (111), (220), and (311) diffraction peaks toward large angles, which indicated a decrease in the lattice parameters due to the substitution of Se for S. The results obtained show that Se atoms can easily replace S with an arbitrary S/Se ratio and form CNTSSe solid solutions. In calculating the unit cell parameter of the CNTSSe solid solution films using FullProf, in the case of using the initial data for a sulfur-based compound, it was found that the a cell constant was 0.551(7) nm. The value obtained was between the values for CNTS (COD no. 00-026-0552, $a = 0.5425$ nm) and CNTSe (COD no. 00-026-0551, $a = 0.57050$ nm). The calculated value of the lattice constant was closer to CNTS because the CNTSSe films contained more sulfur than selenium (Table 1).

In addition, the X-ray diffraction patterns of the CNTSSe films showed reflections from cubic Mo (COD no. 96-901-1607) and trigonal (hexagonal) MoS_2 (COD no. 96-153-5541) that formed during the annealing of precursors in an atmosphere containing chalcogen. X-ray analysis indicated the absence of the MoSe_2 layer in the CNTSSe films. This may indicate that MoS_2 prevents the formation of MoSe_2 . A similar obstacle to the formation of the MoSe_2 layer due to the MoS_2 layer was established in other works during the synthesis of $\text{Cu}_2\text{ZnSn}(\text{S},\text{Se})_4$ thin films by the selenization of deposited Cu/Sn/ZnS precursors by magnetron sputtering on glass/Mo substrates [34,35].

The X-ray diffraction patterns of the CNTSSe films contained a reflection at $2\theta \approx 45.31^\circ$. This peak was not associated with CNTSe and its identification was difficult. Nevertheless, this peak probably belongs to the hexagonal Ni (COD no. 96-901-3008), cubic Se (COD no. 96-901-3135), hexagonal $\text{Ni}_2\text{S}_{1.8}\text{Se}_{0.2}$ (COD no. 96-153-8792), or monoclinic Ni_3Se_4 (COD

no. 96-900-9245) phase. Taking in account the synthesis conditions and the obtained results of EDX mapping images of the CNTSSe films (Figure 5), we can rule out the presence of the pure nickel phase. According to the Crystallography Open Database, the most intense peak from cubic Se (no. 96-901-3135) is at $2\theta \approx 45.45^\circ$. While for hexagonal $\text{Ni}_2\text{S}_{1.8}\text{Se}_{0.2}$ (COD no. 96-153-8792) and monoclinic Ni_3Se_4 , the most intense peak is at $2\theta \approx 34.24^\circ$ and 33.37° , respectively. This may disprove the existence of these phases in the composition of the CNTSSe films. However, according to the COD, the diffraction peak from $\text{Ni}_2\text{S}_{1.8}\text{Se}_{0.2}$ at $2\theta \approx 45.34^\circ$ is the second in intensity and from Ni_3Se_4 at $2\theta \approx 45.18^\circ$ is the third in intensity in diffraction patterns. According to the COD, the strong MoS_2 peak is at 14.5° , and the peak at 40.48° should be more intense than at 33.8° . Considering this, we can conclude that the contribution from the $\text{Ni}_2\text{S}_{1.8}\text{Se}_{0.2}$ or Ni_3Se_4 phase increases the intensity of the peak at $2\theta \approx 30.8^\circ$ compared to the peak at 40.48° belonging to MoS_2 and Mo. The contribution from the MoS_2 phase increases the intensity of the peak by about 45° . This may confirm the formation of the hexagonal $\text{Ni}_2\text{S}_{1.8}\text{Se}_{0.2}$ or monoclinic Ni_3Se_4 phase. In addition, the asymmetric broadening of the peaks at 33.8° and 51.7° may indicate the existence of the Ni_3Se_4 phase along with MoS_2 . In [36], the fabricated nickel foam alloys on the carrier Ni_3Se_4 and Ni_3S_2 were doped with sulfur and selenium, respectively, using a light hydrothermal anion exchange reaction. The samples had a similar surface morphology to the CNTSSe films synthesized in this work. The presence of other impurity phases, for example, $\text{Cu}(\text{S},\text{Se})$, $\text{Sn}(\text{S},\text{Se})$, and $\text{Cu}_2\text{Sn}(\text{S},\text{Se})_3$, in the synthesized CNTSSe films was not found.

The crystallite size (D) of the CNTSSe films was determined from the Scherrer equations as follows [37,38]:

$$D = 0.9\lambda / \beta \cos\theta \quad (1)$$

where λ is the x-ray wavelength; β is the full width of the peak at half maximum (FWHM); θ is the Bragg angle (in radian).

Dislocation density (δ) and microstrain (ε) were calculated using Equations (2) and (3), respectively [38].

$$\delta = 1/D^2 \quad (2)$$

$$\varepsilon = \beta/4\tan\theta \quad (3)$$

The crystallite size, dislocation density, and microstrain for the synthesized films were about 34 nm, 0.00087 nm^{-2} , and 4.2×10^{-3} , respectively. For example, in [37], for the $\text{Cd}_{1-x}\text{Zn}_x\text{S}$ films, the dependence of the electrical conductivity on the grain size was shown, and it was found that the electrical conductivity had a maximum for the film with a grain size of about 36.445 nm ($5 \times 10^{-10} (\Omega \cdot \text{m})^{-1}$). The electrical conductivity of SnS films with crystallites of 55.05 nm is $2.364 \times 10^{-7} (\Omega \cdot \text{cm})^{-1}$ ($\delta = 3.30 \times 10^{14} \text{ m}^{-2}$ and $\varepsilon = 2.31 \times 10^{-3}$) [38].

4. Conclusions

This article presents the results of a study on the morphology and crystal structure of the $\text{Cu}_2\text{NiSn}(\text{S},\text{Se})_4$ (CNTSSe) thin films, which were first obtained by high-temperature annealing of layer-by-layer electrochemically deposited Ni/Cu/Sn/Ni precursors on glass/Mo substrates in chalcogen vapor. The main conclusions can be drawn as follows:

- (1) The Ni/Cu/Sn/Ni precursors had a uniform distribution of the deposited metal layers. The EDX mapping images showed a mutual diffusion of sequentially applied elements, which may indicate the formation of a binary or ternary intermetallic compound in the precursors.
- (2) It has been found that subsequent annealing in chalcogen vapor in air at 580°C for 30 min makes it possible to obtain stable polycrystalline CNTSSe films.
- (3) The CNTSSe films crystallized in a cubic structure. The films had small deviations from stoichiometry in the cation as well as an anion sub-lattice. The diffraction peaks from the CNTSSe on the X-ray patterns were between the positions of the peaks from CNTSe and CNTS. The calculated unit cell parameter for CNTSSe ($a = 0.551(7) \text{ nm}$)

was between the values for CNTSe and CNTS, and was closer to the values for CNTS. This was due to the higher content of sulfur in the films than that of selenium. Using X-ray diffraction, along with the CNTSSe main phase and CNTS phase, the presence of the $\text{Ni}_2\text{S}_{1.8}\text{Se}_{0.2}$ or Ni_3Se_4 phase was detected. No characteristic peaks corresponding to other impurities such as $\text{Cu}(\text{S,Se})$, $\text{Sn}(\text{S,Se})$ or $\text{Cu}_2\text{Sn}(\text{S,Se})_3$ were observed at the detection limit of the XRD apparatus. This shows the phase purity and good quality of the films.

- (4) Annealing of the precursors led to an increase in their thickness from 700 to 900 nm to $\sim 2.4 \mu\text{m}$ due to the insertion of sulfur and selenium atoms in the crystal lattice. It was found that the surface of the CNTSSe films is a homogeneous structure with densely packed large crystals and single pores.

Thus, the obtained results demonstrate the production of the CNTSSe thin films using the proposed method, which can be improved by more precise control of the composition of the initial precursors and heat-treatment conditions.

Author Contributions: Conceptualization, A.V.S., V.V.R., V.F.G., and M.V.G.; Methodology, A.V.S. and T.N.A.; Software, A.V.S., T.N.A., and E.L.T.; Validation, A.V.S., V.V.R., and V.F.G.; Formal analysis, A.V.S., T.N.A., E.L.T., T.I.Z., A.V.T., and S.V.T.; Investigation, A.V.S., T.N.A., and V.V.R.; Resources, A.V.S., T.N.A., E.L.T., T.I.Z., A.V.T., and S.V.T.; Data curation, A.V.S.; Writing—original draft preparation, A.V.S. and T.N.A.; Writing—review and editing, A.V.S., V.V.R., V.F.G., M.V.G., and E.L.T.; Visualization, A.V.S.; Supervision, A.V.S.; Project administration, A.V.S., T.N.A., V.V.R., T.I.Z., A.V.T., and S.V.T.; Funding acquisition, A.V.S., T.N.A., V.V.R., E.L.T., and S.V.T. All authors have read and agreed to the published version of the manuscript.

Funding: This research was financed by the Belarusian Republican Foundation for Basic Research (grant number T21PM-033) and the Russian Foundation for Basic Research (grant number 20-58-04005).

Institutional Review Board Statement: Not applicable.

Informed Consent Statement: Informed consent was obtained from all subjects involved in the study.

Data Availability Statement: Not applicable.

Conflicts of Interest: The authors declare no conflict of interest.

References

- Green, M.A.; Dunlop, E.D.; Hohl-Ebinger, J.; Yoshita, M.; Kopidakis, N.; Hao, X. Solar cell efficiency tables (version 59). *Prog. Photovolt.* **2022**, *30*, 3–12. [[CrossRef](#)]
- Alzahrani, G.S.; Alzahrani, F.S.; Ahmed, M. Nahhas Study of the Specific Factors Effecting the PV Solar Cell's Efficiency in Saudi Arabia. *Sustain. Energy* **2022**, *8*, 6–11. [[CrossRef](#)]
- Moskowitz, P.D.; Fthenakis, V.M. Toxic Materials Released from Photovoltaic Modules During Fires. *Health Risks. Sol. Cells* **1990**, *29*, 63–71. [[CrossRef](#)]
- Green, M.A. Estimates of Te and In prices from direct mining of known ores. *Prog. Photovolt. Res. Appl.* **2009**, *17*, 347–359. [[CrossRef](#)]
- Stanchik, A.V.; Gremenok, V.F.; Juskenas, R.; Tyukhov, I.I.; Tivanov, M.S.; Fettkenhauer, C.; Shvartsman, V.V.; Giraitis, R.; Hagemann, U.; Lupascu, D.C. Effects of selenization time and temperature on the growth of $\text{Cu}_2\text{ZnSnSe}_4$ thin films on a metal substrate for flexible solar cells. *Sol. Energy* **2019**, *178*, 142–149. [[CrossRef](#)]
- Stanchik, A.V.; Tivanov, M.S.; Tyukhov, I.I.; Juskenas, R.; Korolik, O.V.; Gremenok, V.F.; Saad, A.M.; Naujokaitis, A. Temperature dependence of Raman scattering in the $\text{Cu}_2\text{ZnSnSe}_4$ thin films on a Ta foil substrate. *Sol. Energy* **2020**, *201*, 480–488. [[CrossRef](#)]
- Li, X.; Zhuang, D.; Zhang, N.; Zhao, M.; Yu, X.; Liu, P.; Weiab, Y.; Renab, G. Achieving 11.95% efficient $\text{Cu}_2\text{ZnSnSe}_4$ solar cells fabricated by sputtering a Cu–Zn–Sn–Se quaternary compound target with a selenization process. *J. Mater. Chem.* **2019**, *7*, 9948–9957. [[CrossRef](#)]
- Shockley, W.; Queisser, H.J. Detailed balance limit of efficiency of p-n junction solar cells. *J. Appl. Phys.* **1961**, *32*, 510–519. [[CrossRef](#)]
- Tampo, H.; Kim, S.; Nagai, T.; Shibata, H.; Niki, S. Improving the open circuit voltage through surface oxygen plasma treatment and 11.7% efficient $\text{Cu}_2\text{ZnSnSe}_4$ solar cel. *ACS Appl. Mater. Interfaces* **2019**, *11*, 13319–13325. [[CrossRef](#)]
- Taskesen, T.; Neerken, J.; Schoneberg, J.; Pareek, D.; Steininger, V.; Parisi, J.; Gütay, L. Device Characteristics of an 11.4% CZTSe Solar Cell Fabricated from Sputtered Precursors. *Adv. Energy Mater.* **2018**, *8*, 1703295. [[CrossRef](#)]
- Ghosh, A.; Thangavel, R.; Rajagopalan, M. First-Principles Study of Structural Stability and Optical Properties of Cu_2XSnY_4 (X = Fe, Co, Ni; Y = S, Se) for Photovoltaic Applications. *Energy Environ. Focus* **2014**, *3*, 142–151. [[CrossRef](#)]

12. Ozel, F.; Sarilmaz, A.; Istanbulu, B.; Aljabour, A.; Kus, M.; Sonmezoglu, S. Ternary chalcogenides $\text{Cu}_2\text{MSn}(\text{SeS})_4$ ($\text{M} = \text{Zn}^{+2}$ and Co^{+2}) nanocrystals as catalytic materials for efficient counter electrodes in dye-sensitized solar cells. *Sci. Rep.* **2016**, *6*, 29207. [CrossRef] [PubMed]
13. Yüksel, O.F.; Ozel, F.; Akin, Ü.; Tugluoglu, N. Structural, optical and dispersion studies on $\text{Cu}_2\text{NiSn}(\text{SSe})_4$ nanocrystals thin films. *Phys. B Condens. Matter* **2022**, *625*, 413530. [CrossRef]
14. Rondiya, S.; Wadnerkar, N.; Jadhav, Y.; Jadhav, S.; Haram, S.; Kabir, M. Structural, Electronic, and Optical Properties of $\text{Cu}_2\text{NiSnS}_4$: A Combined Experimental and Theoretical Study toward Photovoltaic Applications. *Chem. Mater.* **2017**, *29*, 3133–3142. [CrossRef]
15. Ghosh, A.; Chaudhary, D.K.; Biswas, A.; Thangavel, R.; Udayabhanu, G. Solution-processed Cu_2XSnS_4 ($\text{X} = \text{Fe}, \text{Co}, \text{Ni}$) photo-electrochemical and thin film solar cells on vertically grown ZnO nanorod arrays. *RSC Adv.* **2016**, *6*, 115204–115212. [CrossRef]
16. Khattak, Y.H.; Baig, F.; Soucase, B.M.; Beg, S.; Gillani, S.R.; Ahmed, S. Efficiency enhancement of novel CNTS/ZnS/Zn(O,S) thin film solar cell. *Optik* **2018**, *171*, 453–462. [CrossRef]
17. Hameed, T.A.; Cao, W.; Abdelrazek, E.M.; El Zawawi, I.K.; Mansour, B.A.; Elsayed-Ali, H.E. Effect of substrate temperature on properties of $\text{Cu}(\text{In,Ga,Al})\text{Se}_2$ films grown by magnetron sputtering. *J. Mater. Sci. Mater. Electron.* **2015**, *27*, 3209–3216. [CrossRef]
18. Hameed, T.A.; Cao, W.; Mansour, B.A.; Elzawaway, I.K.; Abdelrazek, E.-M.M.; Elsayed-Ali, H.E. Properties of $\text{Cu}(\text{In,Ga,Al})\text{Se}_2$ thin films fabricated by magnetron sputtering. *J. Vac. Sci. Technol. A Vac. Surf. Film.* **2015**, *33*, 031201. [CrossRef]
19. Volobujeva, O.; Bereznev, S.; Raudoja, J.; Otto, K.; Pilvet, M.; Mellikov, E. Synthesis and characterization of $\text{Cu}_2\text{ZnSnSe}_4$ thin films prepared via a vacuum evaporation-based route. *Thin Solid Films* **2013**, *535*, 48–51. [CrossRef]
20. Broussillou, C.; Viscogliosi, C.; Rogee, A.; Angle, S.; Grand, P.P.; Bodnar, S.; Debauche, C.; Allary, J.L.; Bertrand, B.; Guillou, C.; et al. Statistical Process Control for $\text{Cu}(\text{In,Ga})(\text{S,Se})_2$ electrodeposition-based manufacturing process of $60 \times 120 \text{ cm}^2$ modules up to 14.0% efficiency. In Proceedings of the 42nd Photovoltaic Specialists Conference (PVSC), New Orleans, LA, USA, 14–19 June 2015. [CrossRef]
21. Rosoiu, S.P.; Costovici, S.; Moise, C.; Petica, A.; Anicai, L. Electrodeposition of ternary Sn-Cu-Ni alloys as lead-free solders using deep eutectic solvents. *Electrochim. Acta* **2021**, *398*, 139339. [CrossRef]
22. Kondrotas, R. Electrochemical Deposition of Cu-Zn-Sn Precursor and Formation of $\text{Cu}_2\text{ZnSnSe}_4$ Solar Cell. Ph.D. Dissertar, Vilniaus Universitetas, Vilnius, Lithuania, 2015; 153p.
23. Hansen, R.M. Adherent Electroplating on Molybdenum. Ph.D. Thesis, Newark College of Engineering, Newark, NJ, USA, 1952; 41p.
24. Miettinen, J. Thermodynamic description of the Cu–Ni–Sn system at the Cu–Ni side. *Calphad* **2003**, *27*, 309–318. [CrossRef]
25. Juškėnas, R.; Niaura, G.; Mockus, Z.; Kanapekaitė, S.; Giraitis, R.; Kondrotas, R.; Naujokaitis, A.; Stalnionis, G.; Pakštas, V.; Karpavičienė, V. XRD studies of an electrochemically co-deposited Cu-Zn-Sn precursor and formation of a $\text{Cu}_2\text{ZnSnSe}_4$ absorber for thin-film solar cells. *J. Alloy. Compd.* **2016**, *655*, 281–289. [CrossRef]
26. Copper-Nickel Alloys: Properties, Processing, Applications. Available online: https://www.copper.org/applications/marine/cuni/properties/DKI_booklet.html (accessed on 18 July 2022).
27. Isacfranklin, M.; Yuvakkumar, R.; Ravi, G.; Hong, S.I.; Shini, F.; Thambidurai, M.; Dang, C.; Velauthapillai, D. Marigold flower like structured $\text{Cu}_2\text{NiSnS}_4$ electrode for high energy asymmetric solid state supercapacitors. *Nature Research* **2020**, *10*, 19198. [CrossRef] [PubMed]
28. Dridi, S.; Bitri, N.; Mahjoubi, S.; Chaabouni, F.; Ly, I. One-step spray of $\text{Cu}_2\text{NiSnS}_4$ thin films as absorber materials for photovoltaic applications. *J. Mater. Sci. Mater. Electron.* **2020**, *31*, 7193–7199. [CrossRef]
29. Aitelhaj, D.; Elkissani, A.; Elyagoubi, M.; Aitdads, H.; Welatta, F.; Nkhaili, L.; Chaib, H.; Outzourhit, A. Development of $\text{Cu}_2\text{NiSnS}_4$ based thin film solar cells without a sulfurization step. *Mater. Sci. Semicond. Process.* **2020**, *107*, 104811. [CrossRef]
30. Dehghania, Z.; Shadrokh, Z. Structural and optical properties of $\text{Cu}_2\text{M}(\text{M}: \text{Zn}, \text{Fe}, \text{Co}, \text{Ni})\text{SnSe}_4$ nanoparticles synthesized via heating up method. *Int. J. Light Electron. Opt.* **2018**, *169*, 242–248. [CrossRef]
31. Cui, Y.; Deng, R.; Wang, G.; Pan, D. A general strategy for synthesis of quaternary semiconductor Cu_2MSnS_4 ($\text{M} = \text{Co}^{2+}, \text{Fe}^{2+}, \text{Ni}^{2+}, \text{Mn}^{2+}$) nanocrystals. *J. Dyn. Artic.* **2012**, *22*, 23136. [CrossRef]
32. Yang, C.L.; Chen, Y.H.; Lin, M.; Wu, S.L.; Li, L.; Liu, W.C.; Wu, X.S.; Zhang, F.M. Structural, optical and magnetic properties of $\text{Cu}_2\text{NiSnS}_4$ thin films deposited by facile one-step electrodeposition. *Mater. Lett.* **2016**, *166*, 101–104. [CrossRef]
33. Beraich, M.; Taibi, M.; Guenbour, A.; Zarrouk, A.; Bellaouchou, A.; Fahoume, M. Synthesis of Tetragonal $\text{Cu}_2\text{NiSnS}_4$ Thin Film via Low-Cost Electrodeposition Method: Effect of Ni^{2+} Molarity. *J. Electron. Mater.* **2020**, *49*, 728–735. [CrossRef]
34. Stanchik, A.V.; Baraishuk, S.M.; Zhygulin, D.V.; Pyatlitski, A.N.; Trukhanava, E.L.; Chumak, V.A. Phase composition and microstructure of $\text{Cu}_2\text{ZnSn}(\text{S,Se})_4$ thin films. *Proc. Fr. Skorina Gomel State Univ.* **2021**, *3*, 143–149.
35. Stanchik, A.; Chumak, V.; Trukhanava, E.; Baraishuk, S. Crystal structure and optical properties of $\text{Cu}_2\text{ZnSn}(\text{S,Se})_4$ thin films. *BSPU Bulletin. Ser.* **2021**, *2*, 13–19.
36. Liu, T.; Diao, P.; Lin, Z.; Wang, H. Sulfur and selenium doped nickel chalcogenides as efficient and stable electrocatalysts for hydrogen evolution reaction: The importance of the dopant atoms in and beneath the surface. *Nano Energy* **2020**, *74*, 104787. [CrossRef]

37. Awodugba, A.O.; Ibiyemi, A.A.; Ajayi, J.O. Effect of grain size on the electrical transport mechanism for zinc doped CdS thin films. *Int. J. Sci. Res. Manag. Stud.* **2014**, *1*, 234–241. [[CrossRef](#)]
38. Daniela, T.O.; Unob, U.E.; Isahc, K.U.; Ahmadud, U. Optimization of electrical conductivity of SnS thin film of $0.2 < t \leq 0.4 \mu\text{m}$ thickness for field effect transistor application. *Rev. Mexic. Física* **2021**, *67*, 263–268. [[CrossRef](#)]